Comprehensive investigation on Chalcogenide thin film Coated Multimode Optical Fiber: Visible Evanescent-Wave Absorption Refractometer

[1,2]Z. Heidarnia, [1,2]H. Khoshsima*, [3]R. Parvizi*, [4]H. Heidari

[1]*Faculty of Physics, University of Tabriz, Tabriz 5166616471, Iran*

[2]*Reaserch Institute for Applied Physics and Astronomy, University of Tabriz, Tabriz 5166616471, Iran*

[3]*Department of Physics, College of Sciences, Yasouj University, Yasouj 75914-353, Iran*

[4]*Microelectronics Lab, School of Engineering, University of Glasgow, Glasgow G12 8QQ, United Kingdom*

Abstract:

In this work, a different insight into the absorption characteristics of the chalcogenide thin film over the visible-wavelength range is studied in detailed. A comparative study of the lossy mode resonance (LMR) dips stem from the evanescent-wave absorption is theoretically and experimentally investigated towards refractive index measurement in aqueous environment. The absorbing layer of thermally evaporated arsenic trisulfide chalcogenide (As_2S_3) thin film coated onto the low OH etched optical fiber (ChOF) is prepared. X-ray diffraction (XRD), scanning electron microscopy (SEM), and Raman spectroscopy, were used to characterize the chemical species, the crystal structure, and the morphology of the degradation layer confirming the As_2S_3, thin-film deposition on the curved optical fiber surface. The LMR dips condition hinging on the adoption of the chalcogenide layer was comprehensively explored by referring to the absorption spectra as a function of the wavelength and its thicknesses. Taking the advantage of the chalcogenide absorptive features within the visible spectral range, the results verified that coating even a thin subwavelength thickness of As_2S_3 chalcogenide on a bare has the ability to provide liquid refractometer with a versatile absorbing features. Our results point to a new path for the development of LMR-based chemical sensors, environmental sensors, or to be combined to the integrated micro-photonics device biosensors.

Keywords: As_2S_3 coating, Lossy mode resonance, optical fiber sensor, refractometer.

Introduction

In the last ten years' great attention has been paid to the two-dimensional chalcogenide glasses due to enabling frequency-tunable, optomechanical devices and various medical applications. The chalcogenide glasses based on sulfides are very promising materials for exploited within the various 2–

10 μm infrared spectral device [1-6] due to their transparency in this range and low phonon energies which lead to the shifting of the multi-phonon absorption edge to longer wavelengths[3-7]. In such applications chalcogenide optical fibers have usually been employed utilizing the transparency (glassy) overlay features within Mid-IR region[8, 9]. Higher values of the refractive index and high degree of covalent bonding in chalcogenide increase the probability of radiative transitions in comparison with other basic materials[3, 4]. In this glassy thin-film, unique capability of concentrating light in a small volume for an extended period of time leads to strong enhancement of evanescent field into the interface of sensing layer and surrounding environment[10].

The evanescent wave absorption optical fiber sensor for detecting the refractive index (RI) changes in different chemical substances have been widely used for evaluation of physical parameters, analysis of biological samples and chemical reagents [1-3]. Across the range of the well-known optical sensors, those based on electromagnetic resonances are reliable, robust and highly sensitive relying on the optical properties of the utilized coating thin-films in the sensing region[2]. These resonances give rise to an absorption wavelength band in the output transmitted spectrum that shift in wavelength or altering the intensity when there is a change in the RI of the coating layer or surrounding environment. Basically, the real part of the thin-film permittivity must be negative and higher in magnitude than both its own imaginary part and the permittivity of the surrounding environment [2], SPRs is obtained. However, for the low-reflectance region, the imaginary part is lower and permits the less studied type of resonance based on Lossy Mode Resonances (LMR) as the modes supported by absorbing thin films. As a result this type copes with SPR limitations through introducing an enlarged range of materials for coating from metal oxides, polymers and many other dielectrics [5]. Another important property is that the central wavelength of the LMR can be tuned by using a different coating thickness in the design of an LMR based device.

Recently, some semiconductor oxide based thin films have been applied intensively to fabricate optical fiber based sensors, for example ZnO [11], In_2O_3, WO_3 [12], Al_2O_3 [13]. SnO_2 coated single mode optical fiber also has also been used to study the LMR effect to measure the relative humidity within

near Infra-red region approximately (in the range of 1400-1600), observing the first LMR in 1550 nm and sensitivity of 1.9 nm/%RH [14, 15]. Unlike the mostly of existing researches on Mid IR transparency features of chalcogenide, rarely has been studied the absorption properties of non-crystalline As_2S_3 which was not based on optical fiber [16, 17]. As the calculated average value of optical band gap is about 2.77 eV, which agrees with the experimental measured values of 2.365 eV and 2.2 eV [18], giving rise the absorptive features within the wavelength of green color leading us exploiting this thin film as the sensing layer. Therefore, in this work we concern to study absorptive properties the As_2S_3 sputtered thin-films on multi-mode fiber in the visible light region.

To this end, the layers were coated onto the multi-mode optical fiber and the transmitted light were studied under different refractive index of surrounding aqueous. The dips appeared in the transmitted spectra which can be manipulated by different coating thickness are exploited as underlying factor of determining the refractive index variation of the surrounded environment. Possessing the refractive index of about 2.5, As_2S_3 presents a main advantage of providing a light (evanescent wave) trapping as exposing the interface with the ambient when it is coated on optical fiber (with lower refractive index of 1.45), which in turn results to a versatile portable sensing probe, also we show that this probe has the potential of multiple dips generation in transmitted spectra allowing more accurate measurements. The remainder of this paper is organized as follows.

In Section 2, the depositing and preparing experimental coated optical layer and related setup are explained. The characterization of the coated layers is studied in details and then, the following section analysis on the modeling probe based on the of effective refractive index concept and some rules are given for the design of LMR based sensors. Finally, according to the derived design rules in an evanescent field chemical sensing scenario, the propagation of light trough the coated optical fiber, and the absorption spectra towards sensing performance are studied in detail, for different thicknesses of the coated layer. We believe that this experiments can mainly provide a new avenue of optical biosensing applications.

2. Sensing probe fabrication and sensing architecture

The experimental aspects of this research, such as the coating layers onto the optical fiber, the characterization procedures and measurement setup are described in this section.

The experimental measurement setup basically consists of a halogen-tungsten white light source (SLS251, Thorlabs, Inc.) that dispatches light into the one end of optical fiber and a detector (HR4000CG, UV-NIR, Ocean optics, Inc.) connected to the other end, as shown in Fig. 1 (a). The sensing performance of each as-prepared probe was studied based on the absorption spectrum to measure the refractive index. These fibers were cleaned in piranha solution. Initially, the protective buffer of optical fiber is separated mechanically with a fiber stripper and uncladed by chemically removing with acetone a 1.2 cm part of the polymer cladding then this region is removed by chemical etching by immersion of the fiber in HF acid. The two ends of the chalcogenide coated optical fibers was cleaved and connected to light source and spectrometer by connectors. As shown in Fig. 1, for the fabrication of probes, a multimode plastic-clad silica fiber of numerical aperture 0.40 (FT200EMT, Pure Sillica/TECS Hard cladding, Thorlabs, Inc. 200/225 μm of core/cladding diameter) with 120 mm length was used. A 12 mm cladding at the middle segment of the probe was chemically removed, known as etching process, by immersion of the fiber in a 40% HF acid for use as a sensing area.

Online monitoring of transmitted spectra versus etching time allows us to determine and to control the diameter of the etched fiber, as depicted in Fig. 1 (b). To assess better this effect, during the etching process, the maximum intensity of the transmitted light through the etched fiber is shown in Fig. 1 (b) and for the almost first 5 minutes, the intensity does not change notably. Then, as the fiber becomes thinner, more portion of light leaks out of the fiber in the etched region which would be responsible for sensing reactions. The images of bare fiber and removed clad (etched) one are shown in Fig. 1(b) as the background picture. Before coating the film, it is necessary to explore the speed of etching as shown in Fig. 1 (b), to optimize the leaked light from the etched region (evanescent light) according to the attenuated output power. It means that we have to tradeoff between the leaked light and the transmitted output light intensity. When the etching is more than a critical stage, the fiber become very thin leading to an intensive evanescent wave. On the other hand, it should be noted that the longer etching time

causes a very low intensity of transmitted output light which is not able to recognize properly the variations. Therefore, we have etched optical fiber with time of 41 min and the 57% of light can be transmitted through the etched fiber and the output power experiences nearly 40% loss which is a proper intensity of measurement as our previous works [11, 19]. Then the unclad fibers are placed in a piranha solution for several hours, which removes resistant organic matter from the silica surface and makes the cleaned surface extremely hydrophilic.

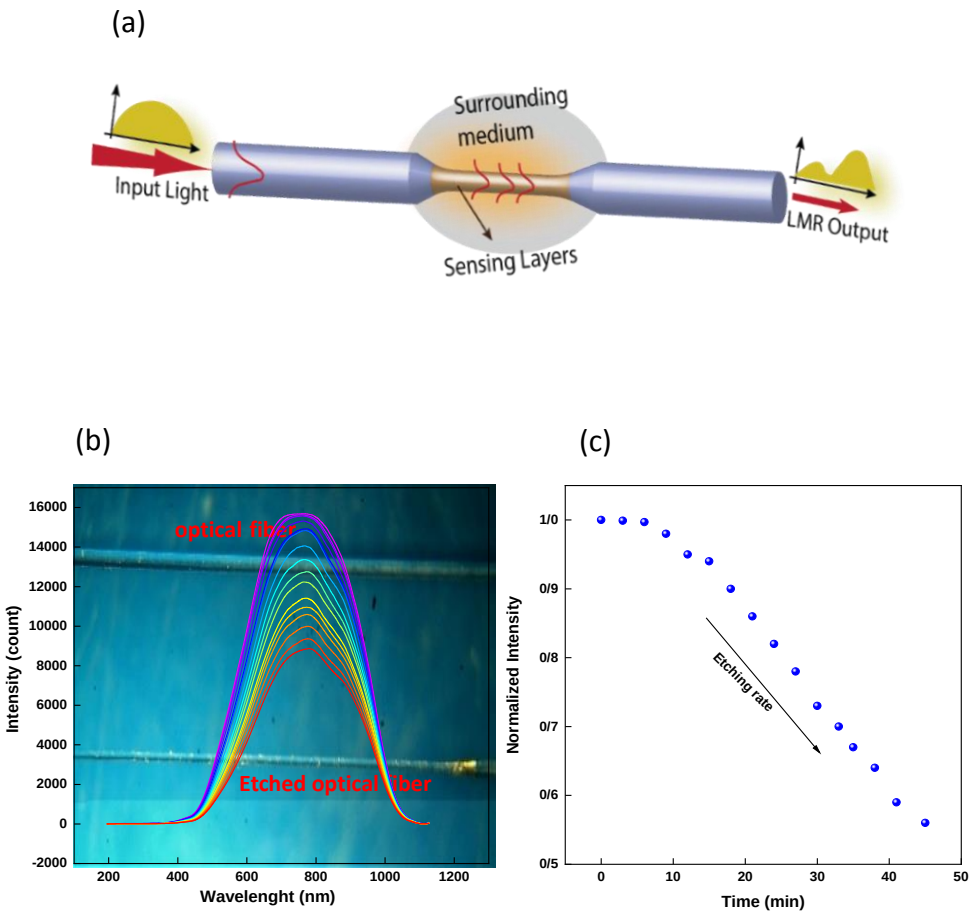

Fig. 1. (a) The schematic diagram of the refractive index measurement optical sensing system, (b) the spectra of the bare fiber immersed into the HF acid recorded every 3 minutes, and images of optical fiber and the etched (clad removed one) in the background image, and (c) the speed of etching optical fiber.

The etched fibers were used as substrates in a sputtering coating process in order to fabricate the thin

homogeneous sensing coating onto the fiber. As_2S_3 coating is done by the thermal evaporation system of this device, which is equipped with a high current power supply and a pair of copper electrodes to perform the coating by thermal evaporation. Various types of boats, baskets or coils (Boat, Basket and coil) can be installed on this system. In this layer, the basket source is used and the suitable current for this material is 14 A, as shown in Fig. 2.

As_2S_3 coatings were fabricated using DST3-T; a three cathode spattering machine from Nano-Structured Coating Co. of England. DST3-T that shown schematically and image in Fig. 2, is a vacuum coater system with a large glass chamber and a turbomolecular pump. The vacuum chamber of the device includes a cylindrical Pyrex with a 300 mm diameter and 250 mm height with L-shaped O-rings. The device is equipped with a high vacuum turbomolecular pump backed by a two-stage rotary pump so that no oil contamination (which is a property of diffusion pumps) enters the vacuum chamber and the coating is performed in a very clean environment. This device is equipped with three water cooled cathodes for sputtering and a thermal evaporation system and with RF and DC power supplies, it is able to coating a wide range of materials including metals (oxide and non-oxide), semiconductors and ceramics. Two quartz crystal thickness gauges are installed inside the chamber, which includes an oscillator and a crystal holder with the ability to measure the thickness during the coating and control the coating rate with one nanometer accuracy.

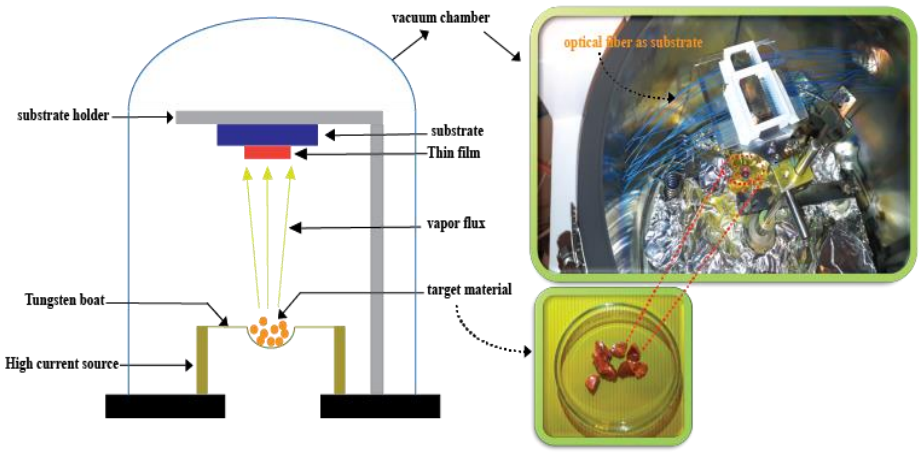

Fig. 2. schematic and image of coating device, with the images of As_2S_3 raw material (shown as target

material) and the chamber including a plexiglass box of arranged optical fibers playing the substrate role.

3. Results and Discussion

3.1 Characterization of the LMR supporting sensitive coatings

Fig. 3 SEM images of As_2S_3, top (a), surface (b) including the insets of cross section and magnified surface of thin-film sputtered onto the optical fiber core, show a homogeneous distribution with low roughness and high uniformity of the film. This figure shows well-layered coating of small nanoparticles on the curved surface of optical fiber (shown in the inset with the magnified scale). The diameter of the etched optical fiber is shown which is about 100 μm meaning the half of the fiber was removed giving rise to the sufficient evanescent wave leakage.

Fig. 3(c) shows the XRD pattern, analyzed by X-ray (X' Pert Pro, of Panalytical Co. with CuKa, k = 1.54 Å) of As_2S_3 layer deposited onto a planar silicon-based substrate. This As_2S_3 thin-film thermally deposited on the SiO_2 planar substrate shows a broadened peak at $2\theta = 20^{\circ}$ denotes the orpiment (As_2S_3) signature without the evidence of the realgar (As_4S_4) presence (peaks appears at $2\theta = 16^{\circ}$) which is in consistent with Raman analysis spectra [20]. XRD pattern indicates the amorphous structure without any distinct extra peak.

Raman scattering was excited (by means of a XploRA Plus from HORIBA Co.) at λ_{exc} = 785 nm for comparative measurements. In Fig. 3(d), Raman spectrum of bulk glass As_2S_3 which has been extensively studied, shows a broad band in the range 250-420 cm^{-1} including a number of various distinctive vibrational modes. It can be observed that a stretching vibration appeared at 306 cm^{-1} assigned to the orpiment of As_2S_3, and the smaller peaks at 199, 221 cm^{-1} seems to be related to As–As bond containing structures which exists even in bulk glass in As_xS_{1-x} [21, 22]. In the spectra of layers with As_2S_3, a weak shoulder of the 353 cm^{-1} band was observed at 367 cm^{-1} (Fig. 3(d)), which might be attributed to the presence of oxygen bonding with arsenic molecules [23]. The presence of As–As bonds requires S–S bonds to occur in As_2S_3 glass network. The Raman peaks related to homopolar S

bonds, which are positioned at 470–495 cm^{-1} as can be seen at this As_2S_3 coated optical fiber spectrum. A broad band extended around vibrational band of ~469 cm^{-1} (dotted lines) which contains a number of various Raman lines stem from S polymeric chains and/or homo polar bonding of S─S [24]. These peaks can be distinctly observed in As_2S_3 layer of the middle spectrum of Fig. 3(c), assigned to the symmetric and anti-symmetric bond stretching vibrational modes of $AsS_{3/2}$ pyramidal units bridged via S atoms to form a quasi-two-dimensional structure (the inset of Fig. 3(c)) with an orpiment-type backbone crystal structure) [25]. According to the Ref [26], adding small quantities of As_2O_3 provided lower loss in the transmitted spectrum of glass optical fibers and showed less effect on the loss for the longer wavelength in the visible region.

In order to study the optical property of the films which is the key feature for LMR realization, the dependence of the transmittance and the regarding absorption spectrum of the film measured by the experimental taken from Diffuse Reflectance Spectroscopy, DRS, analysis for 55 nm glassy As_2S_3 thin-film coated fiber (Fig. 3(e)). The absorption edges of the films are not sharp because these films are amorphous, and possess surface roughness and impurities due to the oxygen vacancies. The imaginary part of the refractive index was taken about 0.02 in visible range absorption adopted from the extracted data reported in the similar literature [16]. In this consideration, the precise agreement of the obtained practical measurement results based on the empirical DRS analysis (Fig. 3(e)) with the reported optical features in that papers were carefully checked.

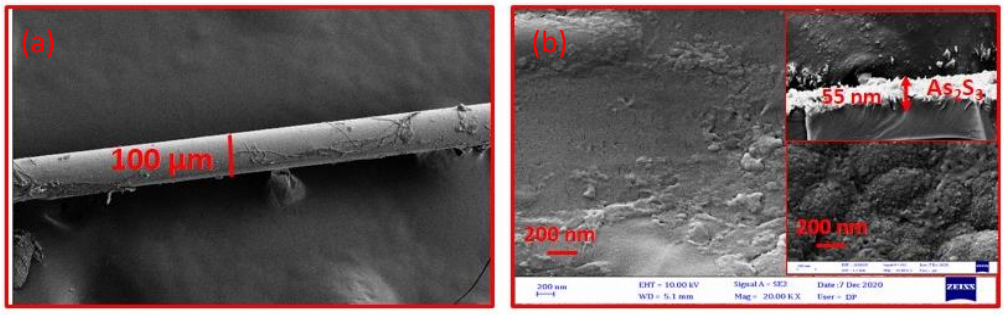

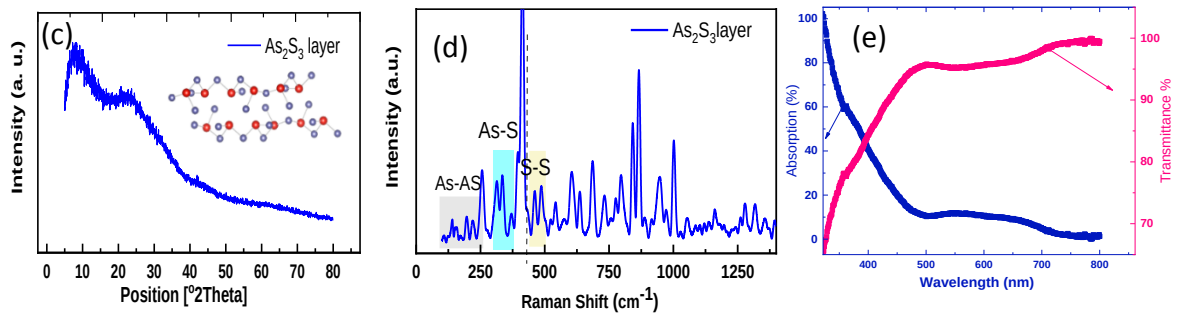

Fig.3 (a, b) SEM image of As_2S_3 in different magnifications, in the up insets are the top and the cross view of As_2S_3, with the insets of magnified images with specified scales. (c) The XRD and (d) Raman spectra of As_2S_3 coated on optical fibers with illustrating the orpiment-type backbone crystal structure of As_2S_3, (e) The absorption and transmittance (Second Y axis data) spectra of as-deposited sensing layers on the optical fiber measured by Diffuse Reflectance Spectroscopy of As_2S_3 thin-film with 55 nm thickness.

3.2 Theoretical background

We first developed a comprehensive theoretical studies through the finite element method (FEM) model to characterize the optical features of the as-proposed chalcogenide coated optical fiber. The essential numerical assessment was carried out via the electromagnetic frequency domain module for two-dimensional modeling from cross section point of view with considering the light propagation along the optical fiber with the z direction, as illustrated in Fig. 4(a). The etched core at 100 µm diameter is taken as pure silica dielectric whose RI is 1.45 and that of cladding is chalcogenide with 55 nm thickness with a real RI of 2.5. Eigenvalues problem is solved of a four layered waveguide structure, e.g. core, coating layer, surrounding solution and lastly, perfectly matched layer (used to prevent reflections back to the calculation region), where the guided light propagates into the core along the z-direction, as shown in Fig. 4 (b). In this case, a 2D region of optical fiber cross section defined the calculation region. Since, the wave shows a type of a slow propagation along the waveguide direction, it is expected more accurate results would be observed by defining the circular shape of fiber as calculation region rather than that of solving 1D slab waveguide along the propagation axis [27].

Transverse electric field distribution, effective refractive index, n_{eff}, are studied in the cross section view of the coated optical fiber. In this calculation, mode analysis technique is used for the fiber where the two different 55 and 240 nm chalcogenide is being taken over the visible wavelength interval. The results supported for 18 number of modes of this structure which is acting as a waveguide are presented in Fig. 4 (C). The remainder of the structure was specified n=1.35 as surrounding environment with immersion solution (refractive index ranging from 1.33 to 1.42 corresponding to the measurements followed section). It is known that the effective refractive index according to the propagation constant of $\beta=n_{eff}k_0$, is different for each mode. The imaginary part of n_{eff} characterizes the losses arising from the coated layer absorption, $\alpha(\omega)=2Im(\beta)$, typically this physical quantity used to inspect the as the refractive index of the environment. To better understand the coupling of propagating light into some higher modes in the coating layer resulting lossy modes [28], the electric field core-guided mode distribution was indicated for every labeled wavelength, .

Dispersion relations of effective index of core mode at solution SRI of 1.35 undergoes a rapid change at a specific wavelength band satisfying the phase matching condition. This attenuated core mode corresponds with the band with the absorption maxima which overcomes the cut-off condition [29]. The results of these calculations for the supported coated thin and thick layers are presented as the lines in Fig. 4 (c) implying the relationship between the imaginary of the mode effective index of modes. The calculations show that the electric fields for the bound and leaky modes over the coating region begins to oscillate and crosses the zero axis at the core and coating layer interface. It can be seen that the field in the 240 nm coating layer adds another cycle of oscillation, which implies that more energy from the core couples to into the higher order modes, less light evanescent out. It is more emphasis on the light trapping within the ticker layer of 240 nm which was shown and compared by images of leaked light of fibers and to focus on the mode distribution of the modes within the core and sensing region, (comparing the figures of S1 & S2). In the thicker layer, the field in the core less confined with emerging higher order modes within core region, implying more energy transfer to the coating chalcogenide layer. We found an insight into the emergence of the possible LMR and its related wavelength through the

2D-based effective refractive index modelling with solving modal parameter Maxwell's governing equations and the z component and the solving process were explained in details in the appendix section. This mode is considered as the first LMR which is appeared within longer wavelength or the lower thickness. More lossy mode guided in the thicker cladding layer of 240 nm deduced from the electric field amplitude decreasing of the bounded core mode which pronounce a more profound absorption feature; accordingly, giving rise the second LMR generation towards shorter wavelength around 560 nm.

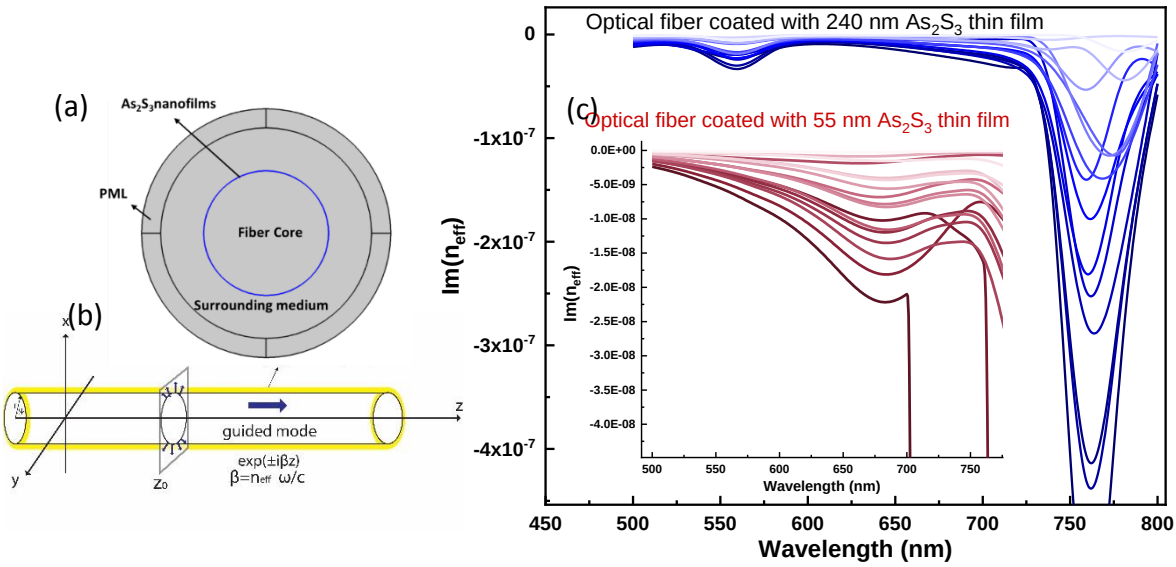

Fig. 4 (a) The cross section of the structure of fiber waveguide, where the etched fiber core is silica with 100 μm diameters. The coated cladding is As_2S_3 nanofilm (displayed with blue color) with considering perfectly matched layer (PML) absorbing boundaries around the structure for wave equations solving. (b) Structure along z with the phase evolving as β in a waveguide. (c) Imaginary part of effective refractive index of 14 modes of 240 nm chalcogenide (with that of 55 nm inside the graph) thin film coated optical fibers.

To better illustrate inner mechanism of the structures, the electric field distributions were depicted and compared at different core guided and highly lossy resonance dips wavelengths. In the case of 55 nm chalcogenide film coated fiber, the indicated electric field distributions (Fig. 5 (a) and (b), Transverse and z component respectively) exhibits the transferred energy from the core modes to lossy mode at wavelength of 55 and 770 nm. In both cases, the field profile at the spectral wavelengths is strongly

confined in the core region, except for the resonance lossy wavelength in which the transmitted light is being depleted. For 55 nm thickness, the guided light was absorbed within a broad wavelength range of more than 770 nm, without indicating an appreciable transmission dip for shorter wavelength. However, for the longer modes of more than 770 nm the modes specially with higher orders clearly are splitting to the slightly and highly lossy waves which are responsible for the dip resonance modes. The properties of slightly lossy modes are close to the core guided modes as it can be seen from (Figs. 5 (a& b)), whereas the characteristics of the highly lossy modes propagated through the overlaying thin film displayed by color intensity appreciably vanishing and blurring inside the core region. The obtained profiles of z component shown in Fig. 5 (d) compares the distribution of the bounded core modes without reshaping with that of and transferring to the lossy layer and low transmitted intensity which is in good agreement with the mentioned results. Consistent with the following experimentally achieved results, these two resonance dips appeared for 240 nm overlay thin film coated fibers, meanwhile the first LMR appeared in the longer wavelength of 750 nm, verifying that more mods transferred to higher orders lossy modes.

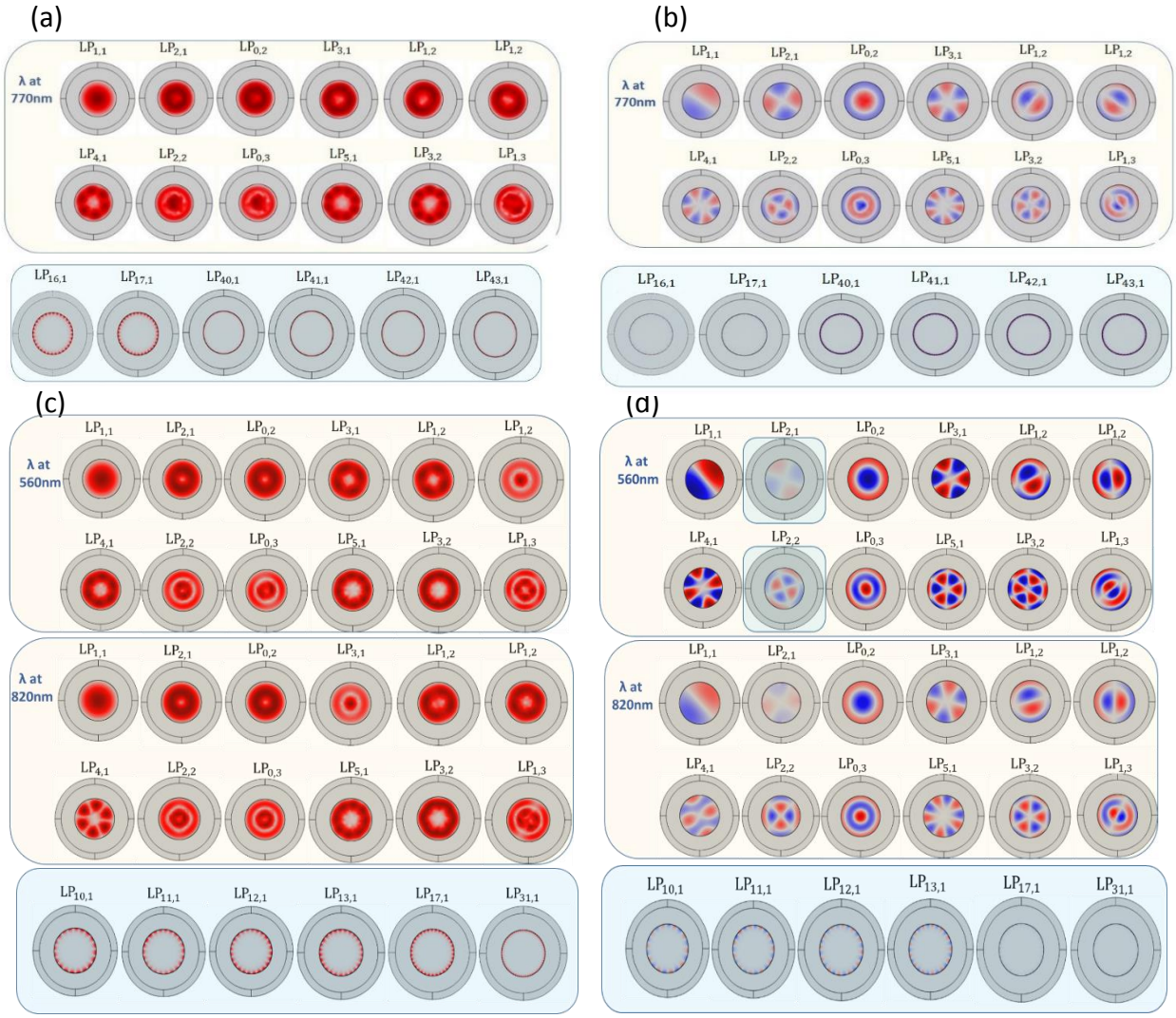

Fig 5. The series of (left side) field and (right side) their related z component profiles of different LP modes at different wavelengths of fibers coated with two thicknesses of (a and b) 55 nm and (c and d) 240 nm coated optical fiber to clearly showing the slightly lossy modes within red box and the highly lossy modes transferring in the blue colored box were displayed, where 770 nm (for 55 nm thickness), the 560 nm and 820 nm (using 240 nm thickness) were corresponding to the two resonance wavelengths.

3.3 Sensing performance experiments

To study the sensing performance, the responses of sensing probes with various thickness listed as 55, 80, 120 and the thicker one of 240 nm were investigated in detail with considering the absorption concept. Generally, the underlying absorption phenomenon is based on the changes on the transmitted

light due to the attenuation stems from environmental variation. Here, the transmission of the light through the sensitive region (called transmittance) represents the relation between the light intensity before and after passing through this sensitive region. We have monitored and recorded the transmitted spectra in exposure to the liquids with a list of surrounding material RI (SMRI)=1.33–1.42. All the coated fibers illustrate the absorbing concept through a separated shifted portion of the spectrum regarding the utilized solution. It can be observed that the dipper but narrower spectra were arousing for thinner thickness of 55 and 80 nm, while the lower transmission dip with a broader special range were immerged for the thicker 120 and 240 nm layers which agrees with the obtained numerical results (Fig. 6).

To more clear and accurate sensing assessment based on the LMR operating principle, the transmitted spectra of probes immersed into the solution were considered with in difference with that of the air exposed as the sensing responses of probes and plotting the calibration curves which it would be discussed in the followings. The transmitted light spectra and corresponding normalized plots (showing the LMR shift in a clearer plot) were indicated against the applying various SMRI as shown in Fig.5. As the SMRI increases, the evanescent wave magnitude enlarges and thus, the guided light intensity through the fiber at the output decreases. This is attributed to this fact that SMRI increasing causes higher effective RI and giving rise to more light attenuation (absorption). Due to the LMR phenomenon attenuation dip occurs at a specific wavelength, λ_R, also changed corresponding to the SMRI increasing. The 55 and 80 nm coated fiber show a well-pronounced characteristic of the dip wavelength shifting specially within refractive index variation of 1.34 to 1.36 is so appreciable, consistent with the obtained numerical results, due to the sufficient phase matching condition of modes for the adequately thin thickness. However, the attenuation and shift at the resonance wavelength is distinctly higher for the sensor probes with depositing the sensitive 120 and 240 nm coating onto the optical fiber, allowing more modes with higher orders transferred to the lossy coating layer. It could be seen that the faint evanescent wave (the light around the sensing region) was emerged for the thickest coating (Fig. 3S).

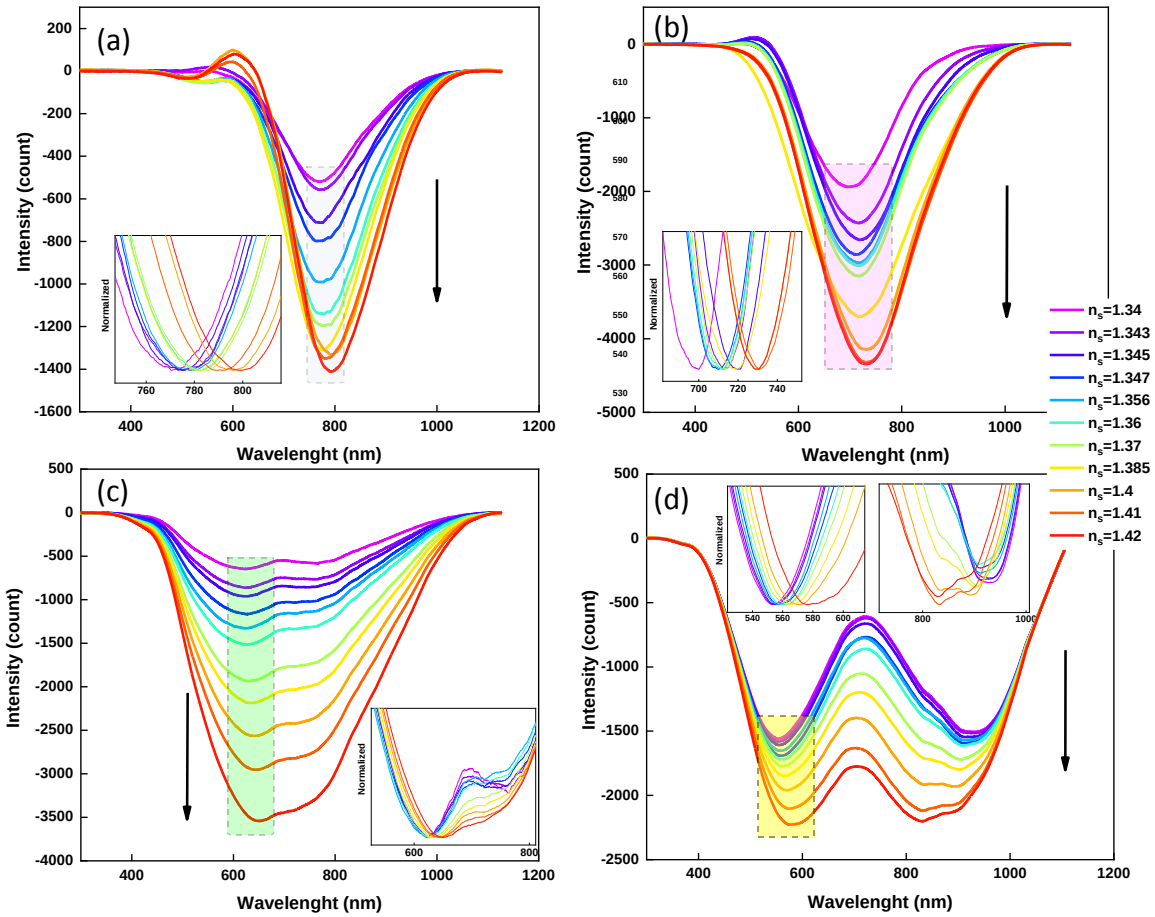

Fig. 6 Transmitted spectra of optical fibers with As2S3 coating, sensing responses of (with the insets in the normalized view) exposed in the various SMRI with different thicknesses with (a) 55, (b) 80, (c) 120 and (d) 240 nm.

The dip wavelength and intensity variation were extracted for the as-prepared optical fibers and plotted in Fig. 7 (a …and d). The thinner coated optical fiber exhibited only one dip of LMR wavelength with a maximum red shift of 135 nm, for the RI change of the sensing aqueous from 1.338 to 1.42. Mostly, the implemented linear fitting indicates two main categories of RI interval of 1.34 to 1.356 and the higher RI of 1.36 to 1.46 displaying a sufficient linearity coefficient within both ranges. The thin film with 80 nm shows the largest dip shifts versus RI changes in the lower RI interval; As_2S_3-based refractometers enable to observe the LMR dips which LMR can be observed with two separated LMR dips in the visible region. It varies linearly with R^2=0.96 and sensing slope of 3919 Δλ/RIU, with increasing SMRI in the wide range of RI=1.33 to 1.4 for the first LMR appeared in the output

transmitted spectra. As the thickness increases the ability of providing multiple dips were clearly observed which becomes well-pronounced utilizing the thickest 240 nm coating layer. Additionally, the decreasing intensity of the coated optical fiber shows a clear exponentially attenuating phenomenon referring to the Langmuier [30] formula.

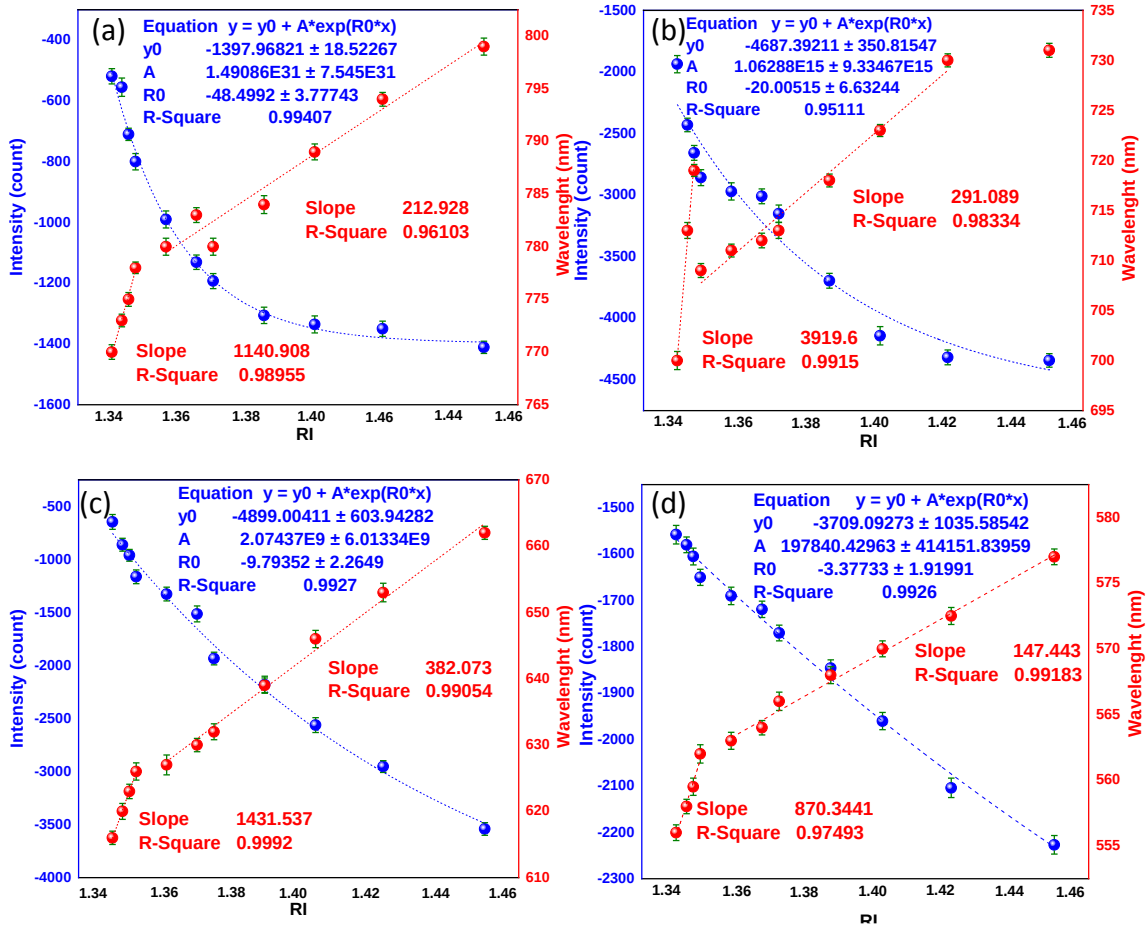

Fig. 7 The dip wavelength extracted for optical fiber coated with different thicknesses of (a) 55, (b) 80, (c) 120 and (d) 240 nm thickness.

As it can be seen, the intensity changes when the external RI change from water to the increased RI solutions and the response of the sensor is very fast and highly repetitive. The intensity of wavelength 672 nm was set to be traced response increased during the successive addition of different SMRI solution. When the sensing probe was immersed in a solution with higher RI, the intensity decreasing, shown in Fig.8, was obtained using as a reference intensity of wet fiber (when the sensor is immersed into water). The intensity of wet fiber slightly decreases for every measurement due to the memory

effect of the successive measurement. It is worth noting that for every main sensing tests which the results were above reported, the probe was washed with water several times with deionized water, then the output was recorded. In this figure, the stability of the probe and the output spectrum was shown and was checked by measuring the absorbance intensity again after every test, which increased when the solution was removed from cell and water was injected into the cell.

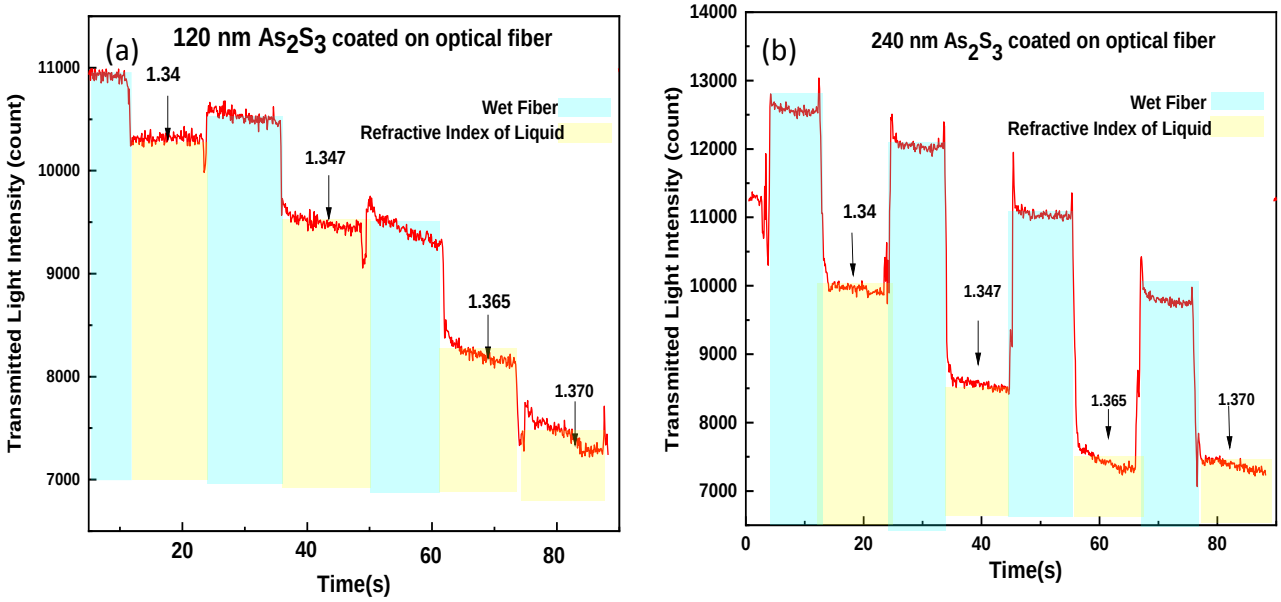

Fig. 8 Variation of intensity attenuation with time as the probe with two different thicknesses of (a) 120 and (b) 240 nm As_2S_3 coated optical fibers were immersed in a solution with higher SMRI and then replaced by water.

Table 1 provides the sensing operations in comparison with the related reported works based on thin-film coated optical fibers responses. This comparison as listed in this table implies that the as-prepared As2S3 coated optical fiber renders versatile and efficient sensing probe able to be exploited for detecting refractive index variation in the aqueous environment.

Table 1. A brief comparison of the sensitivity obtained for LMR-based optical sensors fabricated with different coating materials.

Coating layer	Fiber type	Spectrum range (nm)	SMRI Range	Sensitivity (nm/RIU)	Ref
IGZO	Multimode	600-900	1.32-1.45	1666	[31]
ZnO	Multimode	300-450	1.39-1.43	760	[32]
ITO	Multimode	800-1600	1.32-1.44	1520	[21]
InO_2	Multimode	1100-1600	1.32-1.39	4000	[21]
AZO	Multimode	VIS/NIR	1.3334-1.4471	2280	[19]
ITO	Multimode	900-1500	1.321-1.436	3125	[33]
As_2S_3	Multimode	200-1100	1.34-1.4	3493	This work.

Conclusion

A comparative study of the lossy mode resonance (LMR) dips stem from the evanescent-wave absorption is theoretically and experimentally investigated towards refractometer. The absorbing As_2S_3 thin film coated with different thicknesses onto the low OH etched optical fiber is prepared. we prepared a Lossy Mode Resonances supporting sensitive probe towards refractive index measurement. The morphology, structural and optical properties of the coatings of the sensitive layers were characterized by XRD, Raman, FESEM and DRS analysis confirming the thin-film depositions onto etched low OH optical fibers. Additionally, the enhanced absorbing nature of the as-prepared As_2S_3 coated optical fiber was clarified and validated by the comparison sensor experiments operating based on the both resonance wavelengths shift and intensity attenuation principles. The proposed bilayer coated probe introduces a new path for diverse applications of LMR-based chemical, environmental and bio sensors.

References

[1] E. Udd, W.B. Spillman Jr, Fiber optic sensors: an introduction for engineers and scientists, John Wiley & Sons, 2011.

[2] F. Yang, J. Sambles, Determination of the optical permittivity and thickness of absorbing films using long range modes, Journal of Modern Optics, 44 (1997) 1155-1163.

[3] X. Guo, Surface plasmon resonance based biosensor technique: a review, Journal of biophotonics, 5 (2012) 483-501.

[4] I. Del Villar, V. Torres, M. Beruete, Experimental demonstration of lossy mode and surface plasmon resonance generation with Kretschmann configuration, Optics letters, 40 (2015) 4739-4742.

[5] I. Del Villar, F.J. Arregui, C.R. Zamarreño, J.M. Corres, C. Bariain, J. Goicoechea, C. Elosua, M. Hernaez, P.J. Rivero, A.B. Socorro, Optical sensors based on lossy-mode resonances, Sensors and Actuators B: Chemical, 240 (2017) 174-185.

[6] B.D. Gupta, R. Kant, Recent advances in surface plasmon resonance based fiber optic chemical and biosensors utilizing bulk and nanostructures, Optics & Laser Technology, 101 (2018) 144-161.

[7] O. Fuentes, I. Del Villar, J.M. Corres, I.R. Matias, Lossy mode resonance sensors based on lateral light incidence in nanocoated planar waveguides, Scientific Reports, 9 (2019) 8882.

[8] M.R. Lamont, C.M. de Sterke, B.J. Eggleton, Dispersion engineering of highly nonlinear As 2 S 3 waveguides for parametric gain and wavelength conversion, Optics express, 15 (2007) 9458-9463.

[9] M.R. Lamont, B. Luther-Davies, D.-Y. Choi, S. Madden, B.J. Eggleton, Supercontinuum generation in dispersion engineered highly nonlinear (γ= 10/W/m) As 2 S 3 chalcogenide planar waveguide, Optics Express, 16 (2008) 14938-14944.

[10] D.-G. Kim, S. Han, J. Hwang, I.H. Do, D. Jeong, J.-H. Lim, Y.-H. Lee, M. Choi, Y.-H. Lee, D.-Y. Choi, Universal light-guiding geometry for high-nonlinear resonators having molecular-scale roughness, arXiv preprint arXiv:1909.13594, (2019).

[11] S. Azad, E. Sadeghi, R. Parvizi, A. Mazaheri, M. Yousefi, Sensitivity optimization of ZnO clad-modified optical fiber humidity sensor by means of tuning the optical fiber waist diameter, Optics & Laser Technology, 90 (2017) 96-101.

[12] C. Feng, X. Li, J. Ma, Y. Sun, C. Wang, P. Sun, J. Zheng, G. Lu, Facile synthesis and gas sensing

properties of In2O3–WO3 heterojunction nanofibers, Sensors and actuators B: chemical, 209 (2015) 622-629.

[13] D.J. Mandia, W. Zhou, M.J. Ward, H. Joress, J.J. Sims, J.B. Giorgi, J. Albert, S.T. Barry, The effect of ALD-grown Al2O3 on the refractive index sensitivity of CVD gold-coated optical fiber sensors, Nanotechnology, 26 (2015) 434002.

[14] F.J. Arregui, I. Del Villar, C.R. Zamarreño, P. Zubiate, I.R. Matias, Giant sensitivity of optical fiber sensors by means of lossy mode resonance, Sensors and Actuators B: Chemical, 232 (2016) 660-665.

[15] J. Ascorbe, J. Corres, I. Matias, F. Arregui, High sensitivity humidity sensor based on cladding-etched optical fiber and lossy mode resonances, Sensors and Actuators B: Chemical, 233 (2016) 7-16.

[16] J. Ramirez-Malo, E. Marquez, C. Corrales, P. Villares, R. Jimenez-Garay, Optical characterization of As2S3 and As2Se3 semiconducting glass films of non-uniform thickness from transmission measurements, Materials Science and Engineering: B, 25 (1994) 53-59.

[17] W. Tan, M. Solmaz, J. Gardner, R. Atkins, C. Madsen, Optical characterization of a-As 2 S 3 thin films prepared by magnetron sputtering, Journal of Applied Physics, 107 (2010) 033524.

[18] V. Kaur, S. Tripathi, S. Prakash, Ab initio investigation of optical properties of As2S3 and Ag doped As2S3, Journal of Non-Crystalline Solids, 543 (2020) 120128.

[19] Z. Ashkavand, E. Sadeghi, R. Parvizi, M. Zare, Developed Low-Temperature Anionic 2H-MoS2/Au Sensing Layer Coated Optical Fiber Gas Sensor, ACS Applied Materials & Interfaces, 12 (2020) 34283-34296.

[20] P. Allen, B. Johnson, B. Riley, Photo-oxidation of thermally evaporated As2S3 thin films, J. Optoelectron. Adv. Mater., 7 (2005) 1759-1764.

[21] D. Georgiev, P. Boolchand, K. Jackson, Intrinsic nanoscale phase separation of bulk As2S3 glass, Philosophical Magazine, 83 (2003) 2941-2953.

[22] C. Markos, S.N. Yannopoulos, K. Vlachos, Chalcogenide glass layers in silica photonic

crystal fibers, Optics express, 20 (2012) 14814-14824.

[23] G. Lucovsky, F. Galeener, Local structure and vibrational spectra of v • As2O3, Journal of Non-Crystalline Solids, 37 (1980) 53-70.

[24] S.N. Yannopoulos, F. Kyriazis, I.P. Chochliouros, Composition-dependent photosensitivity in As–S glasses induced by bandgap light: structural origin by Raman scattering, Optics letters, 36 (2011) 534-536.

[25] M. Shastry, M. Couzi, A. Levasseur, M. Ménétrier, Raman spectroscopic studies of As2S3 and Li2S–As2S3 glasses, Philosophical Magazine B, 68 (1993) 551-560.

[26] G. Spierings, Influence of As2O3 on the optical properties of ultrapure multicomponent silicate glasses and optical fibers, Journal of the American Ceramic Society, 67 (1984) 124-127.

[27] S. Khorasani, B. Rashidian, Guided light propagation in dielectric slab waveguide with conducting interfaces, Journal of Optics A: Pure and Applied Optics, 3 (2001) 380.

[28] N. Paliwal, J. John, Sensitivity comparison of LMR based fiber optic refractive index (RI) sensors coated with different materials: Theoretical study, in: Australian Conference on Optical Fibre Technology, Optical Society of America, 2016, pp. AM3C. 6.

[29] I. Del Villar, C.R. Zamarreño, M. Hernaez, F.J. Arregui, I.R. Matias, Generation of lossy mode resonances with absorbing thin-films, Journal of Lightwave Technology, 28 (2010) 3351-3357.

[30] D.F. Santos, A. Guerreiro, J.M. Baptista, Numerical investigation of a refractive index SPR D-type optical fiber sensor using COMSOL multiphysics, Photonic Sensors, 3 (2013) 61-66.

[31] A. Demšar, B. Colarič, S. Rus, J. Lindav, F. Švegelj, B. Orel, B. Praček, A. Zalar, FTIR spectroscopy and AES study of water containment in SiO2 thin films, Thin solid films, 281 (1996) 409-411.

[32] H. Ali, H. Mohamed, S. Mohamed, Enhancement of the optical and electrical properties of ITO thin films deposited by electron beam evaporation technique, The European Physical Journal-Applied Physics, 31 (2005) 87-93.

[33] O. Fuentes Lorenzo, I. Del Villar, J.M. Corres Sanz, I. Matías Maestro, Lossy mode resonance sensors based on lateral light incidence in nanocoated planar waveguides, Scientific Reports,(2019), 9, 8882, (2019).

Appendix:

Since the optical fiber geometry is cylindrically symmetric and also by taking into account that the refractive index only varies with r (n(r)), it is convenient to solve the wave equation based on the cylinderical coordination. As the wave equation for the z component of the field vectors, however, remains more simple :

$$(\nabla^2 + k^2)\begin{pmatrix} E_z \\ H_z \end{pmatrix} \cong 0 \qquad (1)$$

where $k^2 = \omega^2 n^2/c^2$ and ∇^2 is the Laplacian operator in cylindrical coordination which is usually approached by solving for Ez and Hz first and then expressing Er, Eφ, Hr, and Hφ in terms of Ez and Hz. The propagation along the waveguide is considered along the z direction, means that every component of the field vector assumes the same functionality of z- and t-of exp[i(ωt - βz)]. If we follow the Maxwell's equations and equation (1), the problems of wave propagation in a cylindrical structure are usually approached by solving for Ez and Hz first and then expressing E_r, E_φ, H_r, and H_φ in terms of E_z and H_z. Therefore, the z component of electric field is governed by the scalar equation of $\begin{pmatrix} E_z \\ H_z \end{pmatrix} = \Psi(r, \varphi)$ such that

$$(\Delta_T + k_0^2 n^2 - \beta^2)\begin{pmatrix} E_z \\ H_z \end{pmatrix} \cong 0 \qquad (2)$$

The symmetry of the optical fiber is considered by the following equation in cylindrical coordinates rather than Cartesian ones:

$$\frac{\partial^2 \Psi(r,\varphi)}{\partial r^2} + \frac{1}{r}\frac{\partial \Psi(r,\varphi)}{\partial r} + \frac{1}{r^2}\frac{\partial^2 \Psi(r,\varphi)}{\partial \varphi^2} + [k_0^2 n^2(r) - \beta^2]\Psi(r,\varphi) = 0 \qquad (3)$$

We look for separable solutions, which are the product of radial and azimuthal variations:

$$\Psi(r,\varphi) = R(r)\Phi(\varphi) \qquad (4)$$

. They should therefore fulfill the following equation

$$\Phi\frac{d^2R}{dr^2} + \Phi\frac{1}{r}\frac{dR}{dr} + R\frac{1}{r^2}\frac{d^2\Phi}{d\varphi^2} + [k_0^2 n^2(r) - \beta^2]R\Phi = 0 \qquad (5)$$

which, divided by $\frac{R\Phi}{r^2}$, can be cast in the following form:

$$\frac{r^2}{R}\frac{d^2R}{dr^2} + \frac{r}{R}\frac{dR}{dr} + r^2[k_0^2 n^2(r) - \beta^2] = -\frac{1}{\Phi}\frac{d^2\Phi}{d\varphi^2} \qquad (6)$$

. To reach a reasonable point, a necessary condition is that $\frac{1}{\Phi}\frac{d^2\Phi}{d\varphi^2} = \text{constant}$, the Φ function can be derived as

$$\frac{1}{\Phi}\frac{d^2\Phi}{d\varphi^2} = l^2 \rightarrow \frac{d^2\Phi}{d\varphi^2} = l^2\Phi \qquad (7)$$

i.e., that solutions are combinations of $e^{\pm l\varphi}$, and thus, due to periodicity, *l* is an integer, taken as positive. For any value of $l \geq 1$; we find two independent solutions: $\Phi(\varphi) = \cos(l\varphi)$ and $\Phi(\varphi) = \sin(l\varphi)$. and for each one of them, two orthogonal polarization states are possible introducing mode with corresponding *l* number. Once l has been determined, the left-hand side provides the radial variations of the field:

$$\frac{r^2}{R}\frac{d^2R}{dr^2} + \frac{r}{R}\frac{dR}{dr} + r^2[k_0^2 n^2(r) - \beta^2] = l^2 \qquad (8)$$

The $R(r)$ function is obtained, for each value of l, by solving Eqn. (8). It is actually convenient to normalize this equation using the normalized frequency:$V = k_0 a\sqrt{n_1^2 - n_2^2}$ the transverse propagation constants. This equation is solved within the whole structure defined in Fig. 3 (A) with considering the continuity and boundary condition and defining for every specific region with the substituting the regarding refractive index as: inside the core, $u^2 = K_1^2 - \beta^2$, where $k_1 = \frac{2\pi n_1}{\lambda} = \omega\sqrt{\varepsilon_1\mu}$, and in the coated thin film $W^2 = \beta^2 - K_2^2$, where $K_2 = \frac{2\pi n_2}{\lambda} = \omega\sqrt{\varepsilon_2\mu}$, and the similar definition for the surrounding medium. The obtained results of the electric field distribution of z component were illustrated for some specific wavelengths implying the mode transfer as shown (Fig. 4 (B)and explained in the text.